Long-Term Validation of Rapid Impedance Spectrum Measurements as a Battery State-of-Health Assessment Technique

SAE 2013 World Congress

Jon P. Christophersen
John L. Morrison
Chester G. Motloch
William H. Morrison

April 2013

Idaho National Laboratory

SAE International®

Long-Term Validation of Rapid Impedance Spectrum Measurements as a Battery State-of-Health Assessment Technique

Jon P. Christophersen
Idaho National Laboratory

John L. Morrison
Montana Tech. of Univ. of Montana

Chester G. Motloch
Motloch Consulting, Inc.

William H. Morrison
Montana Tech. of Univ. of Montana

ABSTRACT

The objective of this study was to assess the long-term capability and impact of a rapid, in-situ impedance measurement technique known as Harmonic Compensated Synchronous Detection. This technique consists of a sum-of-sines excitation signal that includes a targeted selection of frequencies and only requires one period of the lowest frequency. For a given frequency range of 0.1 Hz to approximately 2 kHz, the measurement duration would only be ten seconds. The battery response is captured and synchronously detected for impedance spectra measurements. This technique was compared to laboratory-based performance degradation measurements using commercially available lithium-ion cells. The cells were aged for 150,000 cycles at accelerated rates using temperatures of 40 and 50°C. Every 30,000 cycles, cycle-life testing was interrupted to gauge degradation at the reference temperature of 30°C. The results demonstrated that growth in the ohmic and charge transfer resistances during aging strongly correlate with the corresponding changes in discharge capacity, pulse resistance, and available power capability that were independently determined from standardized test methods. Additionally, the rapid impedance spectrum technique appears to be a benign measurement that does not impact battery aging. Consequently, this technique appears to be useful as an onboard sensor that, when combined with passive measurements, may be used for enhanced diagnostics, management, and control.

INTRODUCTION

Batteries and other energy storage devices are becoming increasingly important for several industries, including automotive, electric utilities, and military applications. For example, electric, hybrid, and plug-in-hybrid electric vehicles are placing higher demands on the battery packs for engine-off modes, as well as enhanced power assist for motive function to reduce fuel consumption. Batteries are also experiencing increasing power and energy requirements for portable military and commercial electronics, such as radios and computer systems. Battery technologies must perform in normal as well as severe environments, such as military combat missions that may include temperatures ranging from −40°C to 50°C in military aircraft [1], or have a 15-year calendar life, as in the case of U.S. commercial hybrid electric vehicles [2,3]. These performance requirements, combined with the high costs of energy storage devices, emphasize the need for improved battery management systems that accurately assess the overall state-of-health and remaining useful life in addition to optimized management, control, and safety.

Typical management systems focus on passive measurements of voltage and current as a function of time and temperature to gauge battery health [4,5,6]. A smart system uses the measured data to count coulombs while also compensating for degradation losses (e.g., using a weighting factor to compensate for efficiency losses). These can also require periodic full discharges and charges to assess overall remaining capacity as a function of use and to recalibrate the system [4]. Alternatively, the remaining capacity could be estimated based on equivalent circuit models that track the changes in the main charge storing capacitor element using a sliding-mode observer and Kalman estimator techniques [5]. Other methods include offline testing to establish lookup tables that can be used in combination with expert learning systems to assess the state-of-health (SOH) from passive measurements. For example, Okoshi et al. developed lookup tables of SOC versus direct current resistance for vehicle idling-stop-system applications, and incorporated Kalman filtering techniques to predict SOH based on direct current measurements [6]. However, simple passive monitoring provides an incomplete picture of health and this forces manufacturers to oversize their battery designs which increases costs. With higher demands on battery technologies, improved health assessment techniques are required for enhanced management systems that can extend life, increase performance capability, improve safety, and provide useful information for secondary use applications (e.g., an automotive battery at end of life that could be used for grid stabilization).

Electrochemical Impedance Spectroscopy (EIS) has been shown to be a valuable laboratory tool for battery diagnostics. The acquired spectra can reveal changes in the bulk behavior of the electrochemical processes as the battery ages, which can give an indication of deterioration in the electrode surface and diffusion layer [7]. Parameters extracted from impedance spectra, such as the ohmic and charge transfer resistances, have been incorporated into many modeling tools (physics-based, empirical, and semi-empirical models) for offline estimations of battery performance and overall life capability [7,8,9]. Although EIS has not generally been considered for online sensing (historically, the measurement time can be lengthy and the required equipment is typically bulky and expensive), rapid impedance spectra measurement techniques have been developed using a simplified hardware platform that could be designed as an embedded system [10-11]. These techniques could be implemented as an onboard sensor that, when combined with passive measurements, may be used for enhanced battery diagnostics, management, and control. A prototype SOH assessment architecture based on the rapid impedance measurement techniques for onboard battery management systems is presently under development [12].

EXPERIMENTAL

The purpose of this study was to assess the long-term capability and impact of a rapid, in-situ impedance measurement technique known as Harmonic Compensated Synchronous Detection (HCSD). The HCSD technique consists of a sum-of-sines excitation current signal that includes frequencies separated by octave harmonics so as to eliminate the effects of crosstalk interference. With no crosstalk error, the duration of the excitation signal needs to be only one period of the lowest frequency. Thus, given a frequency range of 0.1 to 1638.4 Hz with 15 frequencies included within the sum-of-sines excitation signal, the measurement duration would only be ten seconds long. Each of the harmonic frequencies would include multiple periods to fill the ten-second measurement duration (e.g., the first harmonic of 0.2 Hz would have two periods within the sum-of-sines, the next harmonic of 0.4 Hz would have four periods, etc.). The overall battery response to the excitation signal is captured and then synchronously detected at each frequency of interest to determine the impedance spectrum [10].

Long-term validation of HCSD was conducted on commercially available, high-power lithium-ion cells having a layered oxide cathode with Nickel Manganese Cobalt (NMC) and graphite anode [13]. The cells are 18650-size and have a rated capacity of 1.2 Ah. Several of these cells were subjected to aging protocols for the purpose of validating the Plug-in Hybrid Electric Vehicle (PHEV) testing methodology [3]. As part of that effort, 25 cells were characterized and then subjected to life aging at various temperatures using the test matrix shown in Table 1 [13]. Characterization testing was performed at a reference temperature of 30°C, beginning with a sequence of constant current discharges from a fully charged state. The first three discharges were performed at the one-hour rate (i.e., 1.2 A) to ensure cycling stability. This was followed by a constant power discharge test and a low-current Hybrid Pulse Power Characterization (L-HPPC) test. The constant power discharge test is a scaled, 10-kw discharge between the maximum and minimum voltages. The cells had a scaling factor of 1400, so the constant power test was performed at 7.14 W [13]. The L-HPPC test profile is shown in Figure 1, and consists of 10-s discharge and regen pulses with a 40-s rest at open circuit voltage in between [3]. This profile is repeated at each 10% depth of discharge (DOD) increment starting at 90% state-of-charge. After the L-HPPC, a 25-hour static capacity test was performed using a constant current of 48 mA (i.e., 1.2 A / 25) between the maximum and minimum voltages. Finally, the cells were characterized with an EIS measurement at 15% DOD over a frequency range of 100 kHz to 0.01 Hz with ten points per decade of frequency.

Table 1. Control group test matrix for PHEV validation testing.

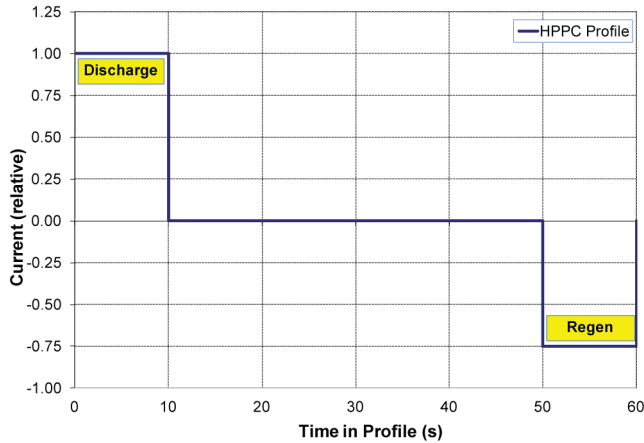| Group	# of Cells	Temperature	SOC
1	10	30°C	60%
2	5	40°C	60%
3	5	50°C	60%
4	5	60°C	60%

Figure 1. HPPC profile that is repeated at each 10% DOD increment [3].

Long-term aging for these cells consisted of cycle-life testing using the 50-Wh PHEV charge-sustaining test profile that is shown in Figure 2. This constant power profile is scaled to meet the cell requirements (using a factor of 1400 in this case) and was repeated continuously at the designated temperature and state-of-charge (SOC) from Table 1. Cycling was interrupted every 30,000 cycles for reference performance tests (RPTs) to gauge cell degradation as a function of aging. Reference performance tests consisted of a scaled, 10-kW constant power discharge and L-HPPC test at 30°C. Every fifth RPT, a 25-hour static capacity test and an EIS measurement at 15% DOD were also included [13].
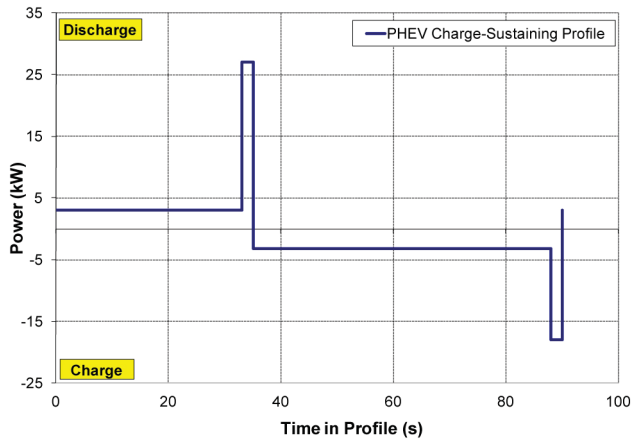

Figure 2. Charge sustaining cycle-life test profile [3].

The acquired test data from Table 1 have been discussed by Belt et al. [13] and were used as a control group for this HCSD validation study. Portions of the control group matrix in Table 1 were duplicated using twelve fresh cells with the addition of HCSD measurements at each RPT. The test matrix is shown in Table 2, and consists of accelerated aging at 40 and 50°C. As with the control group, the HCSD study cells were cycled at 60% SOC based on the PHEV charge-sustaining profile (see Figure 2) with RPTs every 30,000 cycles. Groups A and C in Table 2 were intended to verify the effectiveness of HCSD measurements under no-load conditions. Six cells (i.e., three cells per temperature group) were subjected to the same testing regime as the control group, but with the addition of an HCSD measurement at 60% SOC at characterization and every RPT immediately prior to the start of each cycle-set. Groups B and D in Table 2 included HCSD measurements every RPT as well, but were also subjected to ten thousand HCSD measurements while under active cycling to determine the impact of impedance measurements under load.

Table 2. Test matrix for HCSD validation study.

Group	# of Cells	Temperature	SOC	Comment
A	3	40°C	60%	No-Load Only
B	3	40°C	60%	Under Load
C	3	50°C	60%	No-Load Only
D	3	50°C	60%	Under Load

RESULTS AND DISCUSSION

The cells were aged for 150,000 cycles at the designated test temperature and SOC, resulting in seven HCSD measurements under no-load conditions as the cells degraded (characterization, end of life, and every RPT in between). The input sum-of-sines current for the rapid impedance spectra measurements covered a frequency range of 0.1 to 1638.4 Hz in octave harmonics with one period of the lowest frequency (i.e., 10 seconds) using a excitation current of 0.5 A_{RMS}. The cells with measurements under load (i.e., Groups B and D in Table 2) were each subjected to a total of 10,000 HCSDs during life testing as well. Impedance spectra results from the under load studies will be discussed in a separate publication.

Performance Degradation

Figure 3 shows a comparison of the average pulse resistance growth (determined from the L-HPPC test) between the HCSD study cells and the corresponding control groups at 60% SOC. The average control group results are shown by the open symbols, and the HCSD groups are in solid symbols. At first glance, these data appear to indicate that the HCSD cells have less degradation than the corresponding control cells. However, the average resistances for the HCSD cells are also lower at Characterization and RPT0 (i.e., the RPT immediately prior to first cycle set). This indicates the presence of manufacturing variability for the

cells, which may affect both the magnitude of the measured degradation parameter (e.g., capacity, resistance, and power) and the rate of degradation. For better comparisons, the HCSD average data were normalized to the corresponding control group results at RPT0 since that is the typical point of reference for gauging cell growth during life testing [2,3,9].
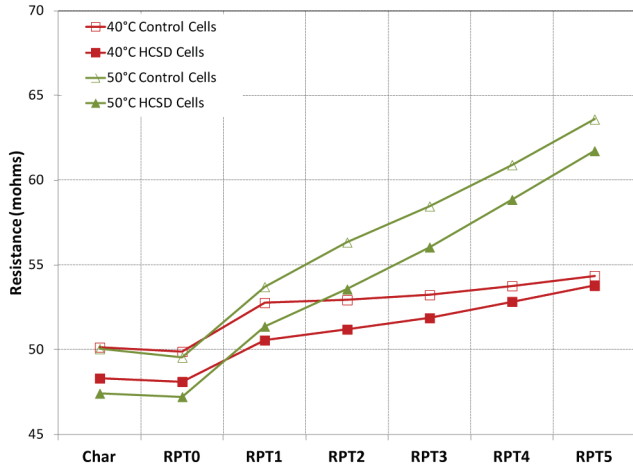

Figure 3. Pulse resistance comparison between control groups and HCSD groups.

Capacity

The normalized average discharge capacity fade for the HCSD groups under (a) no-load and (b) load conditions through RPT5 is summarized in Table 3 and shown in Figure 4. For both the no-load and load HCSD groups, the normalized irreversible capacity loss between Characterization and RPT0 is less than the corresponding control groups. This may indicate that the solid electrolyte interphase layer for the cells assigned to the HCSD groups were not as well formed, and it could also have deleterious effects on the resistance growth and power fade rates as well [14]. Beyond RPT0, the capacity degradation rate for the HCSD groups at each temperature appears very similar to the corresponding control groups for both the no-load and load conditions. The average capacity fade for the HCSD groups, however, is generally less than the corresponding control groups. Furthermore, as shown in Table 3, the average capacity for the HCSD cell group under load is within one standard deviation of the no-load group at both 40 and 50°C. These data, therefore, imply that there is no impact from HCSD measurements on the cell capacity degradation.

Table 3. Average discharge capacity summary for the control and normalized HCSD groups.

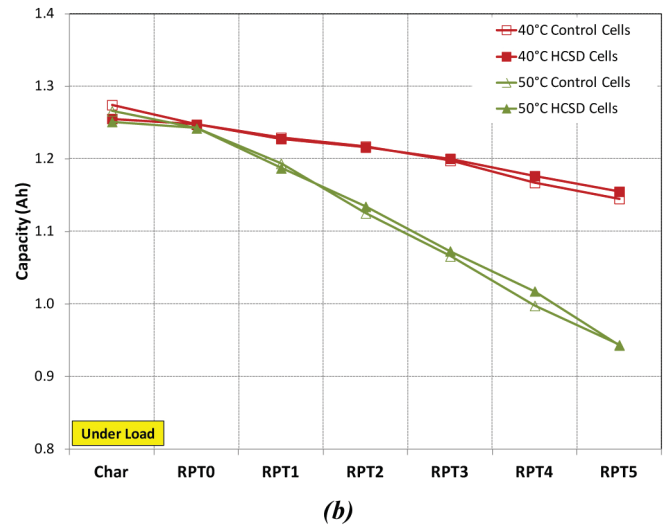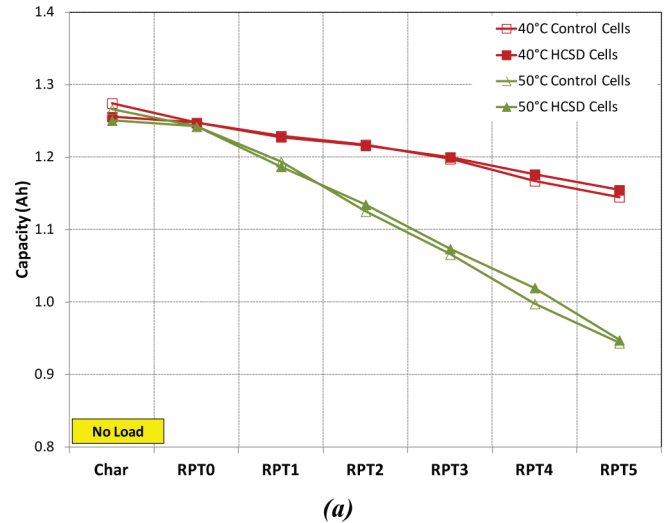| Temp.	Group	RPT0 (Ah)	RPT5 (Ah)	%-Change
40°C	Control	**1.247 ± 0.002**	**1.145 ± 0.003**	**8.19 ± 0.13**
	No-Load	1.247 ± 0.004	1.155 ± 0.005	7.40 ± 0.09
	Load	1.247 ± 0.001	1.154 ± 0.002	7.43 ± 0.10
50°C	Control	**1.242 ± 0.007**	**0.943 ± 0.026**	**24.05 ± 1.75**
	No-Load	1.242 ± 0.003	0.943 ± 0.001	24.07 ± 0.10
	Load	1.242 ± 0.003	0.947 ± 0.008	23.72 ± 0.46

(a)

(b)

Figure 4. Normalized average capacity loss for the HCSD cells under (a) no-load and (b) load conditions.
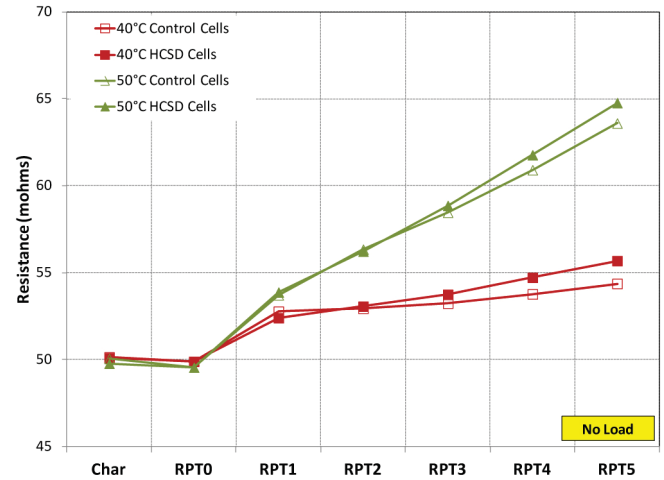
Pulse resistance

The normalized average discharge pulse resistance at 60% SOC for the HCSD groups under (a) no-load and (b) load conditions through RPT5 is summarized in Table 4 and shown in Figure 5. The rate of resistance growth for the HCSD groups is higher than the corresponding control

groups, but the source of this increased degradation does not appear to come from the in-situ impedance measurements. If HCSD measurements had a detrimental impact on cell degradation, then the rate of degradation would increase with both the temperature and the number of measurements. However, as shown in Table 4, the difference between the average resistance for the HCSD and control groups at 40°C is about the same as the difference at 50°C after RPT5 (i.e., approximately 1.2 mΩ, or 2.5%), which indicates no temperature effect. Additionally, the no-load and load HCSD groups showed similar degradation rates through five cycle-sets. The no-load cells were subjected to only seven HCSD measurements at the voltage corresponding to 60% SOC; the load cells were subjected to an additional 10,000 measurements during cycle-life testing. Despite the significantly larger set of in-situ impedance measurements, the HCSD cells under load conditions did not show any accelerated degradation compared to the no-load cells (i.e., both cell groups showed almost 12% and 31% resistance growth at 40 and 50°C, respectively, after five cycle sets).

HCSD measurements, therefore, do not appear to have an impact on discharge resistance growth. The larger degradation observed for the HCSD cell groups could be due to an improperly formed solid electrolyte interphase layer between Characterization and RPT0, as observed with the capacity degradation (see Figure 4). An additional variable is the cell manufacturing variability (see Figure 3). Finally, test equipment and measurement variability may have also contributed to the differences observed in Figure 5 [15-16]. For example, the average temperature at 60% SOC during the L-HPPC test was consistently cooler for the HCSD cells compared to the control group (i.e., between 0.5 to one degree lower) because different environmental chambers were used during the testing. The effect of temperature on lithium-ion cells has been previously documented [9], and lower temperatures generally yield higher resistance values. This is consistent with the observed resistance behavior of the HCSD cell groups.

Table 4. Average discharge pulse resistance summary for the control and normalized HCSD groups.

| Temp.	Group	RPT0 (mΩ)	RPT5 (mΩ)	%-Change
40°C	Control	**49.89 ± 0.36**	**54.37 ± 0.20**	**8.98 ± 0.44**
	No-Load	49.89 ± 0.55	55.84 ± 0.55	11.94 ± 0.28
	Load	49.89 ± 0.26	55.68 ± 0.24	11.61 ± 0.10
50°C	Control	**49.55 ± 0.36**	**63.59 ± 2.16**	**28.36 ± 4.88**
	No-Load	49.55 ± 0.52	64.77 ± 0.78	30.71 ± 0.39
	Load	49.55 ± 0.14	64.77 ± 0.10	30.71 ± 0.41

(a)
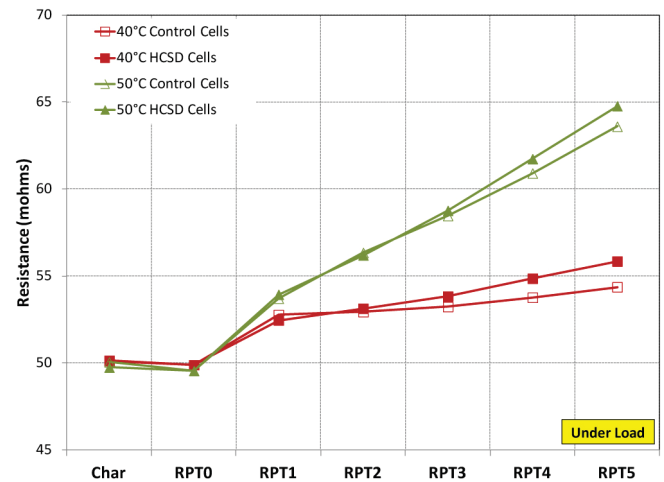
(b)

Figure 5. Normalized average pulse resistance growth for the HCSD cells under (a) no-load and (b) load conditions.
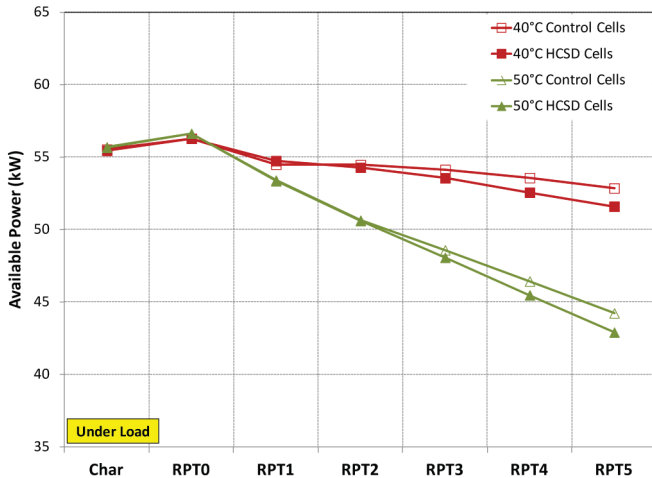
Available power

The normalized average Available Power at 500 Wh (as defined in [3]) for the HCSD groups under (a) no-load and (b) load conditions through RPT5 is summarized in Table 5 and shown in Figure 6. The 50°C cells reached end-of-life after 150,000 cycles since the available power dropped below the target of 45 kW [3]. As expected, the available power mirrors the discharge resistance behavior in Figure 5. The power fade also appears unaffected by the number of HCSD measurements since the no-load and load groups at each temperature condition are within one standard deviation of each other at RPT5. Furthermore, the difference between the HCSD and control groups is consistent for each temperature (approximately 1.2 kW, or 2.2%). The power-fade data, therefore, also implies that there is no impact from long-term HCSD measurements under both no-load and load conditions.

Table 5. Average available power summary at 500 Wh for the control and normalized HCSD groups.

Temp.	Group	RPT0 (kW)	RPT5 (kW)	%-Change
40°C	Control	**56.27 ± 0.37**	**52.85 ± 0.20**	**6.08 ± 0.28**
	No-Load	56.27 ± 0.70	51.59 ± 0.49	8.31 ± 0.39
	Load	56.27 ± 0.19	51.69 ± 0.18	8.14 ± 0.13
50°C	Control	**56.62 ± 0.43**	**44.23 ± 1.39**	**21.87 ± 2.85**
	No-Load	56.62 ± 0.53	42.91 ± 0.51	24.22 ± 0.30
	Load	56.62 ± 0.19	43.05 ± 0.12	23.96 ± 0.41
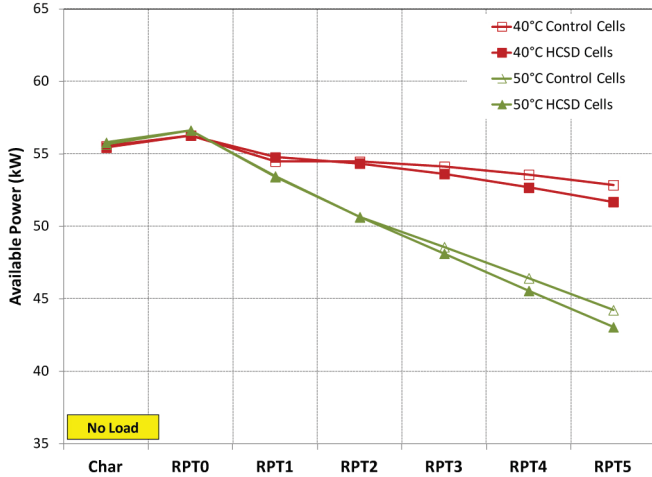
(a)

(b)

Figure 6. Normalized average available power at 500 Wh for the HCSD cells under (a) no-load and (b) load conditions.

Impedance Spectrum Measurements

A representative Nyquist curve from an HCSD measurement at characterization is shown in Figure 7. As the cell ages, both the ohmic (R_O) and charge transfer resistances (R_{CT}) increase, although the majority of the growth is generally with R_{CT} [10]. A simple approach for gauging increase in both the ohmic and charge transfer resistance due to cell aging is to monitor the growth at the semicircle trough, which is the transition point between the charge transfer resistance and Warburg tail, as indicated in Figure 7. The low-frequency Warburg tail is typically unaffected by cell aging when measured under no-load conditions and merely shifts to the right as the ohmic and charge transfer resistances increase.
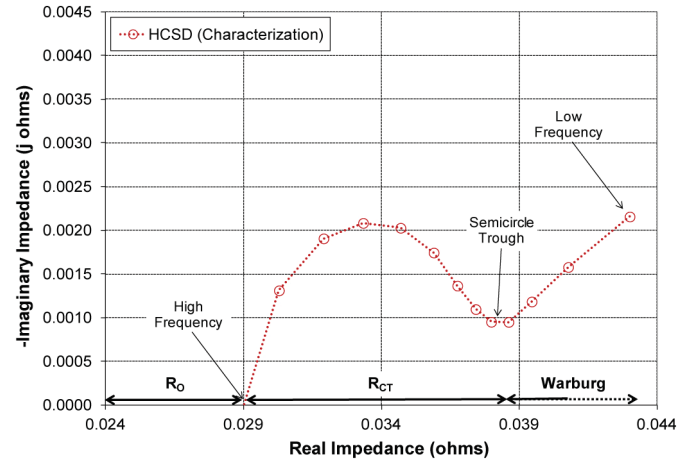

Figure 7. Impedance spectrum from HCSD.

HCSD measurements

All four cell groups in Table 2 were subjected to HCSD measurements at the open-circuit voltage corresponding to 60% SOC as part of the RPT sequence. Figure 8 shows the resulting average HCSD impedance spectra for the: (a) 40; and (b) 50°C cells, respectively, under no-load conditions through five cycle-sets. In all cases, the impedance at RPT0 (solid diamond symbols) is smaller than at Characterization (solid circle symbols), and this is likely due to cell formation. After RPT0, both the ohmic and charge transfer resistance in the mid-frequency region grew with increasing cycle-sets, and the rate of growth was higher at 50°C, as expected. For the load groups (not shown), the cells were subjected to an additional 2,000 HCSD measurements during each cycle-set between RPTs, but this did not appear to affect the rate of impedance growth. Table 6 summarizes the average real impedance measured at the semicircle trough through RPT5. For a given test temperature, both the no-load and load groups are within one standard deviation of each other after 150,000 cycles; this is true of the percent-change in resistance between RPT0 and RPT5 as well. These results are consistent with the observed degradation from the L-HPPC performance data (see above), and also imply that in-situ HCSD impedance measurements do not have an impact on cell performance.
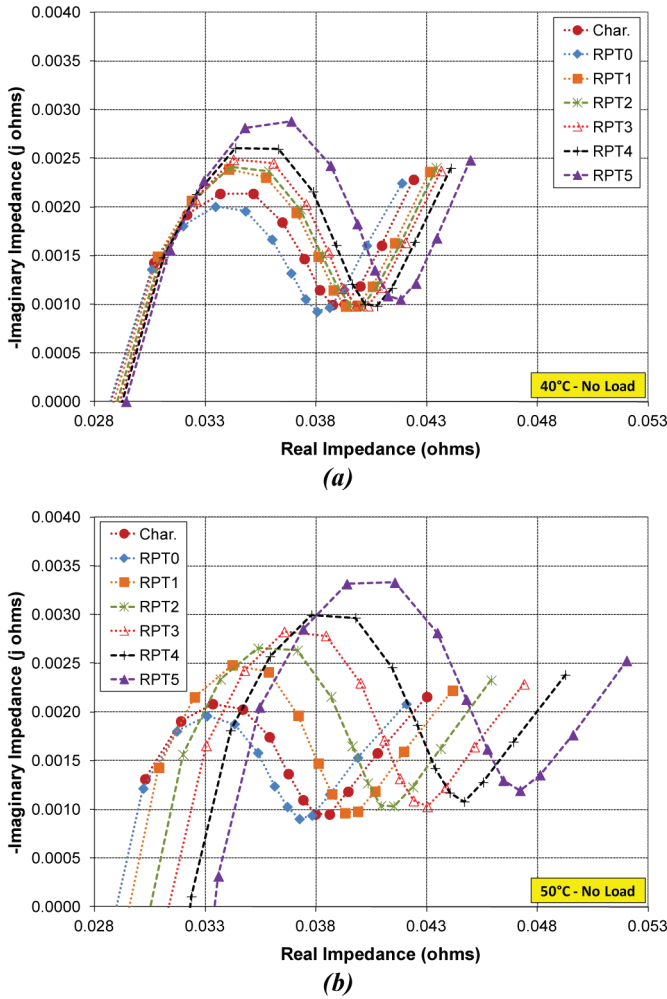
(a)

(b)

Figure 8. Average HCSD measurements at (a) 40°C and (b) 50°C for the no-load conditions through RPT5.

Table 6. Average real impedance at the semicircle trough.

Temp.	Group	RPT0 (mΩ)	RPT5 (mΩ)	%-Change
40°C	No-Load	38.05 ± 0.19	41.83 ± 0.25	9.92 ± 0.14
	Load	38.14 ± 0.61	41.95 ± 0.46	9.99 ± 0.60
50°C	No-Load	37.25 ± 0.17	47.23 ± 0.12	26.80 ± 0.27
	Load	37.47 ± 0.52	47.17 ± 0.65	25.91 ± 0.81

EIS measurements

The four cell groups in Table 2 were also subjected to EIS measurements at 60% SOC at Characterization and RPT5. Figure 9 shows the average EIS measurements for the no-load cells at: (a) 40; and (b) 50°C, respectively, with open symbols. The corresponding average HCSD impedance spectra, normalized to the EIS ohmic resistance, are also shown with solid symbols. The spectra at RPT5 were artificially shifted on the real axis (i.e., the abscissa) for clarity, so the axis labels have been removed. As expected,

both the HCSD and EIS impedance spectra show growth in the charge transfer resistances at RPT5. The HCSD impedance tends to consistently under-predict the reactance, and also appears to have a larger semicircle width. These discrepancies, however, are primarily caused by the system calibration, and improved techniques have recently been implemented that show good preliminary results [17]. Despite these differences, both the EIS and HCSD measurements show similar growth rates in charge transfer resistance.
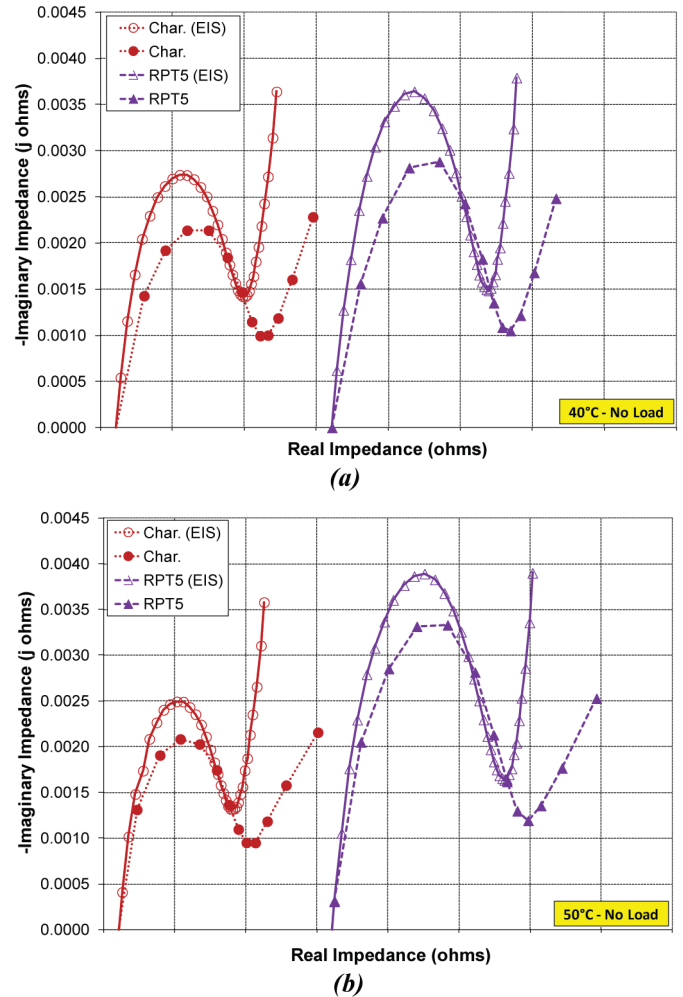

(a)

(b)

Figure 9. Average HCSD and EIS measurements at (a) 40°C and (b) 50°C for the no-load conditions through RPT5.

Tables 7 and 8 summarize the growth in average real impedance at the semicircle trough based on the EIS and HCSD measurements, respectively, between Characterization and RPT5 (the HCSD measurements in this case were not normalized to the EIS results). For each temperature group, the EIS and HCSD results are generally within one standard deviation of each other. Furthermore, the measured impedance values at the semicircle trough determined from EIS were at similar frequencies to the corresponding HCSD results. At Characterization, the EIS trough frequency for the

twelve cells generally ranged between 1.26 and 1.60 Hz, and the corresponding HCSD results were between 0.8 and 1.6 Hz. Likewise, at RPT5, the EIS trough frequencies were generally at 1 Hz, and the corresponding HCSD results were at 0.8 Hz. Therefore, these data indicate that ten-second HCSD measurements under no-load conditions can accurately reflect standardized EIS results, which can take anywhere between ten minutes to an hour to complete depending on system settings.

Table 7. Average EIS real impedance at the semicircle trough.

Temp.	Group	RPT0 (mΩ)	RPT5 (mΩ)	%-Change
40°C	No-Load	39.03 ± 0.73	42.09 ± 0.47	7.85 ± 0.83
	Load	39.04 ± 0.21	42.00 ± 0.23	7.58 ± 0.07
50°C	No-Load	38.25 ± 0.54	46.91 ± 0.60	22.66 ± 0.63
	Load	38.02 ± 0.32	47.02 ± 0.29	23.70 ± 0.39

Table 8. Average HCSD real impedance at the semicircle trough.

Temp.	Group	RPT0 (mΩ)	RPT5 (mΩ)	%-Change
40°C	No-Load	39.11 ± 0.45	41.82 ± 0.24	6.93 ± 1.11
	Load	38.78 ± 0.67	41.95 ± 0.46	8.17 ± 0.73
50°C	No-Load	38.41 ± 0.62	47.22 ± 0.12	22.96 ± 1.69
	Load	38.65 ± 0.78	47.16 ± 0.65	22.03 ± 1.89

Correlations

To gauge the effectiveness of the HCSD technique as a measure of cell degradation, the growth in the charge transfer resistance from the HCSD measurement can be compared to the independently determined change in capacity, pulse resistance, and available power. Figure 10 shows the average HCSD real impedance at the semicircle trough plotted against the measured discharge capacity from the scaled, 10-kW constant power discharge test (i.e., the results from Figure 4). Parameter values from the linear regression fits are summarized in Table 9. These data show a strong relationship with a correlation coefficient of 0.97 or higher. There is a small temperature dependence between capacity fade and impedance growth, but there is no apparent affect from the 10,000 HCSD measurements that were performed for the cells under load conditions. These data indicate that the HCSD technique could be used as an indicator of capacity degradation during aging as an adjunct to coulomb counting techniques.
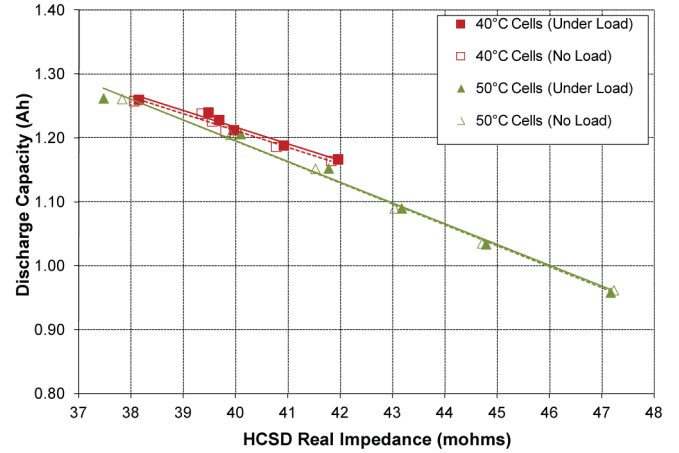

Figure 10. HCSD real impedance correlated to the scaled 10-kW constant power discharge capacity.

Table 9. Trendline fit for the HCSD vs. scaled 10-kW constant power discharge capacity.

Temp.	Group	Slope	Intercept (Ah)	r^2
40°C	No-Load	-0.026	2.262	0.968
	Load	-0.026	2.252	0.970
50°C	No-Load	-0.033	2.504	0.997
	Load	-0.033	2.497	0.989

Figure 11 shows the average HCSD real impedance at the semicircle trough plotted against the L-HPPC discharge pulse resistance at 60% SOC (i.e., the results from Figure 5). Parameter values from the linear regression fits are summarized in Table 10. As shown, these data are also highly correlated (r^2 >0.94), and the growth in HCSD real impedance is about 1.5 times faster than the corresponding L-HPPC data, regardless of test temperature and number of in-situ impedance measurements during cycling. Thus, HCSD impedance measurements under no-load conditions can also accurately reflect the growth in L-HPPC pulse resistance as a function of cell age.

Table 10. Trendline fit for the HCSD vs. L-HPPC discharge pulse resistance.

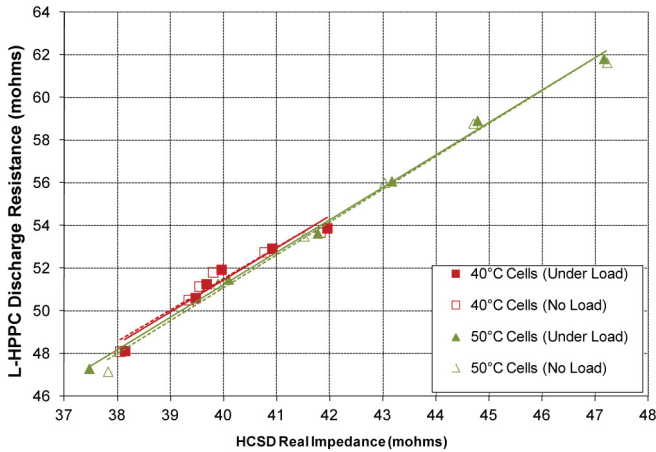| Temp.	Group	Slope	Intercept (mΩ)	r^2
40°C	No-Load	1.469	-7.267	0.946
	Load	1.503	-8.674	0.954
50°C	No-Load	1.543	-10.635	0.992
	Load	1.520	-9.587	0.997

Figure 11. HCSD real impedance correlated to the L-HPPC discharge pulse resistance.
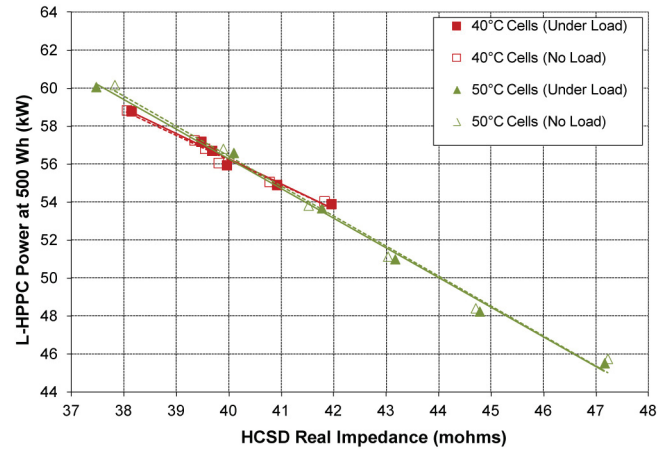

Figure 12. HCSD real impedance correlated to the L-HPPC available power at 500 Wh.

Figure 12 shows the average real impedance at the semicircle trough plotted against the L-HPPC Available Power at 500 Wh (i.e., the results from Figure 6). Parameter values from the linear regression fits are summarized in Table 11; the slopes are negative because power is inversely proportional to the resistance. These data show a strong correlation as well (r^2 >0.98), and still appear independent from the number of in-situ impedance measurements during cycling. However, there seems to be a small temperature dependence in this case as well, and this may be due to the fact that available power is a derived parameter that is based on a combination of the calculated pulse power capability and cumulative energy removed [3]. Since both the power capability and energy removed are independently affected by temperature during the L-HPPC test, the overall temperature effect may be amplified when compared to a directly measured parameter, such as the HCSD impedance. Nevertheless, these data demonstrate that the HCSD impedance is also a very good indicator of power fade as a function of cell age.

Table 11. Trendline fit for the HCSD vs. L-HPPC available power at 500 Wh.

Temp.	Group	Slope	Intercept (kW)	r²
40°C	No-Load	-1.298	108.110	0.981
	Load	-1.317	108.934	0.983
50°C	No-Load	-1.578	119.529	0.991
	Load	-1.561	118.720	0.994

SUMMARY/CONCLUSIONS

HCSD measurements under no-load conditions were conducted at 60% SOC for all cell groups in this study as part of the RPT sequence. From the resulting impedance spectra, the charge transfer resistance in the mid-frequency region grew with increasing cycle-sets, and the rate of growth was higher for the 50°C cells. The rate of impedance growth for the cells subjected to 10,000 HCSD measurements while under load was similar to the no-load cells with only seven impedance measurements in each temperature group, further indicating that HCSD measurements do not impact cell degradation. Although HCSD impedance spectra showed some slight differences compared to standardized EIS measurements, the rate of impedance growth was similar for both EIS and HCSD through five months of aging at accelerated rates. Additionally, the growth of the charge transfer resistance (as reflected in the real impedance measured at the semicircle trough) strongly correlates with both the independently measured capacity, pulse resistance, and available power capability. Therefore, HCSD impedance measurements under no-load conditions appear to accurately reflect degradation as a function of aging without affecting cell life as a result of the measurement.

REFERENCES

1. Naval Air Warfare Center Aircraft Division. *Performance Specification-Batteries, Storage, Aircraft: General Specifications For; MIL-PRF-8565K*, 2001.
2. *FreedomCAR Battery Test Manual for Power-Assist Hybrid Electric Vehicles, DOE/ID-11069.* 2003.
3. *Battery Test Manual for Plug-In Hybrid Electric Vehicles, Revision 2, INL/EXT-07012536.* 2010.
4. Kurle W.D., Johnson S.B., Nordness R.W., Firman S.L., Gustavson D.M., Choi P.Y.. *Smart Battery With Maintenance and Testing Functions. U.S. Patent 6,072,299* June 6, 2000.
5. Gould C.R., Bingham C.M., Stone D.A., Bentley P.. *New Battery Model and State-of-Health Determination Through Subspace Parameter Estimation and State-Observer Techniques.* 2009, IEEE Trans. Veh. Technol., Vol. 58 (8), pp. 3905-3916.
6. Okoshi T., Yamada K., Hirasawa T., Emori A.. *Battery condition monitoring (BCM) technologies about lead-acid batteries.* 2006, J. Power Sources, Vol. 158, pp. 874-878.

7. Kozlowski J.D.. *Electrochemical cell prognostics using online impedance measurements and model-based data fusion techniques.* 2003. Proceedings from the IEEE Aerospace Conference, Vol. 4. pp. 3257-3270.

8. Schalkwijk W.A. van, Scrosati B. [ed.]. *Advances in Lithium-Ion Batteries.* New York: Kluwer Academic/Plenum Publishers, 2002.

9. Christophersen J.P., Bloom I., Thomas E.V., Gering K.L., Henriksen G.L., Battaglia V.S., Howell D.. *Advanced Technology Development Program for Lithium-Ion Batteries: Gen 2 Performance Evaluation Final Report, INL/EXT-05-00913*, 2006.

10. Christophersen, J., Morrison, J., Morrison, W., and Motloch, C., "Rapid Impedance Spectrum Measurements for State-of-Health Assessment of Energy Storage Devices," *SAE Int. J. Passeng. Cars - Electron. Electr. Syst.* 5(1):246-256, 2012, doi:10.4271/2012-01-0657.

11. Christophersen J., Morrison J., Rose D., Morrison W., Motloch C.. *Crosstalk Compensation for a Rapid, Higher- Resolution Impedance Spectrum Measurement*, IEEE Aerospace Conference Proceedings, 2012.

12. Garcia H. E., Mohanty A., Christophersen J. P., Lin W., *On-line State-of-Health and Remaining-Useful-Life Assessment of Batteries using Rapid Impedance Spectrum Measurements*. 45th Power Sources Conference Proceedings, 2012.

13. Belt J., Utgikar V., Bloom I.. *Calendar and PHEV Cycle Life Aging of High-Energy, Lithium-Ion Cells Containing Blended Spinel and Layered-Oxide Cathodes*, 2011, J. Power Sources, Vol. 196, pp. 10213-10221.

14. Balbuena P.B., Wang Y., [ed.]. *Lithium-Ion Batteries: Solid Electrolyte Interphase*. London: Imperial College Press, 2004.

15. *Uncertainty Study of INEEL EST Laboratory Battery Testing Systems Volume 1: Background and Derivation of Uncertainty Relationships*, INEEL/EXT-01-00505. 2001.

16. *Uncertainty Study of INEEL EST Laboratory Battery Testing Systems Volume 2: Application of Results to INEEL Testers*, INEEL/EXT-01-00505. 2003.

17. Morrison W., Morrison J., Christophersen J., Bald P.. *An Advanced Calibration Procedure for Complex Impedance Spectrum Measurements of Advanced Energy Storage Devices.* 58th International Instrumentation Symposium Proceedings, 2012.

CONTACT INFORMATION

Jon P. Christophersen, PhD.
Corresponding Author
Idaho National Laboratory
PO Box 1625
Idaho Falls, ID 83415-2209
Jon.Christophersen@inl.gov

John L. Morrison, PhD.
Montana Tech of the University of Montana
1300 W. Park
Butte, MT 59701
jmorrison@mtech.edu

Chester G. Motloch, PhD.
Motloch Consulting, Inc.
725 West Riverview Dr.
Idaho Falls, ID 83401
cmotloch@gmail.com

William H. Morrison
Montana Tech of the University of Montana
1300 W. Park
Butte, MT 59701
morrison.theta.sigma@gmail.com

ACKNOWLEDGMENTS

DEFINITIONS/ABBREVIATIONS

DOD - depth of discharge

EIS - electrochemical impedance spectroscopy

HCSD - harmonic compensated synchronous detection

L-HPPC - low-current hybrid pulse power characterization

NMC - Nickel Manganese Cobalt

PHEV - Plug-in hybrid electric vehicle

R_{CT} - charge transfer resistance

R_O - ohmic resistance

RPT - reference performance test

SOC - state of charge

SOH - state of health